PHYSICAL REVIEW E **93**, 052901 (2016)

Pattern transition, microstructure, and dynamics in a two-dimensional vibrofluidized granular bed

Istafaul H. Ansari and Meheboob Alam*

Engineering Mechanics Unit, Jawaharlal Nehru Center for Advanced Scientific Research, Jakkur P.O., Bangalore 560064, India

(Received 4 January 2016; published 9 May 2016)

Experiments are conducted in a two-dimensional monolayer vibrofluidized bed of glass beads, with a goal to understand the transition scenario and the underlying microstructure and dynamics in different patterned states. At small shaking accelerations ($\Gamma = A\omega^2/g < 1$, where A and $\omega = 2\pi f$ are the amplitude and angular frequency of shaking and g is the gravitational acceleration), the particles remain attached to the base of the vibrating container; this is known as the solid bed (SB). With increasing Γ (at large enough shaking amplitude A/d) and/or with increasing A/d (at large enough Γ), the sequence of transitions/bifurcations unfolds as follows: SB ("solid bed") to BB ("bouncing bed") to LS ("Leidenfrost state") to "2-roll convection" to "1-roll convection" and finally to a gas-like state. For a given length of the container, the coarsening of multiple convection rolls leading to the genesis of a "single-roll" structure (dubbed the *multiroll transition*) and its subsequent transition to a granular gas are two findings of this work. We show that the critical shaking intensity ($\Gamma^{\rm LS}_{\rm BB}$) for the BB $\rightarrow$ LS transition has a power-law dependence on the particle loading ($F = h_0/d$, where h_0 is the number of particle layers at rest and d is the particle diameter) and the shaking amplitude (A/d). The characteristics of BB and LS states are studied by calculating (i) the coarse-grained density and temperature profiles and (ii) the pair correlation function. It is shown that while the contact network of particles in the BB state represents a hexagonal-packed structure, the contact network within the "floating cluster" of the LS resembles a liquid-like state. An unsteadiness of the Leidenfrost state has been uncovered wherein the interface (between the floating cluster and the dilute collisional layer underneath) and the top of the bed are found to oscillate sinusoidally, with the oscillation frequency closely matching the frequency of external shaking. Therefore, the granular Leidenfrost state is a period-1 wave as is the case for the BB state.

DOI: 10.1103/PhysRevE.93.052901

I. INTRODUCTION

The earliest scientific work on pattern formation in granular media dates back to Chladni [1] and Faraday [2], who studied the now well known heaping phenomenon in shallow layers of vibrating particles. There has been a renewed interest in understanding the pattern-formation scenario in a vibrated granular bed starting from the early 1990s [3–32], and two comprehensive reviews on granular patterns till 2005 can be found in Refs. [33,34]. Since then a vertically shaken box of particles has become a canonical experimental setup to study granular patterns; more specifically, under harmonic shaking via $y(t) = A\sin(2\pi f t)$, such a system is known to admit a variety of interesting patterns: the standing waves, f/n subharmonic waves via period-doubling bifurcations [3,13,30], surface waves and heaping [4,6], Faraday waves and "oscillons" [16,18], convection [5,7,10,11], and the density-inverted state [26,31]. The primary control parameter for the onset and/or bifurcation of any of these patterns is the dimensionless shaking acceleration $\Gamma = A\omega^2/g$, which is a relative measure of the driving acceleration with respect to the gravitational acceleration g. For a review on various patterns in a quasi-2D vibrated bed as well as to know the specific contributions of various research groups, we refer the readers to the introductory section of a recent work [35]. In the present experimental work, we shall primarily focus on unveiling the transition scenario among different patterns (the bouncing bed, the density-inverted state, the convection and the granular gas) in a vibrofluidized bed with increasing Γ, and this being a well-studied problem, here we provide only a brief review of the recent works [31,36,37] which motivated the present study.

The above mentioned density-inverted state was dubbed the *granular* Leidenfrost state (LS) by Eshuis *et al.* [31], who established a possible connection with the original Leidenfrost effect [38]: a liquid drop placed on a hot plate can float over its own vapor layer if the temperature of the plate exceeds a minimum value (Leidenfrost temperature). Akin to this, a dense, compact layer of particles can be supported by a dilute gaseous region of fast moving particles underneath it in a vertically shaken granular bed beyond the critical value of the shaking intensity. More specifically, they found that a dense region of particles with crystalline-type structure can float over a granular gas at mild acceleration ($\Gamma \sim 10$) which bifurcates from a time-periodic bouncing bed state. Previous molecular dynamics (MD) simulations had also predicted the possibility of such *density inversion* [8] or *floating cluster* [26] in a similar setup.

The most recent and comprehensive experimental work of Eshuis *et al.* [36], on shallow vertically shaken granular materials held in a quasi-2D box (of a few particles wide), provides the complete phase diagram of various patterns consisting of (i) a solid bed, (ii) a bouncing bed, (iii) subharmonic undulatory waves, (iv) the granular Leidenfrost state, (v) convection, and (vi) granular gas. They also carefully documented the related bifurcation scenario for each pattern as a function of Γ and the particle loading. They found that with increasing shaking intensity Γ the convection rolls can appear either (i) from the bouncing-bed state at small particle loading, or (ii) from the Leidenfrost state at large particle loading. On the other hand, the primary onset of the Leidenfrost state was found to occur from the undulatory waves with increasing Γ;

*meheboob@jncasr.ac.in

however, the undulatory state can also exist over a range of Γ between two Leidenfrost states (at lower and higher values of Γ). The latter finding implies that two successive bifurcations from a "subharmonic" wavy state to the Leidenfrost state resulted in the onset of convection at large particle loadings. It must be noted that the temporal order of the Leidenfrost state was never quantified [31,36,37,39] via experiments, but it appears to be a quasisteady or steady state from the related theoretical analyses [35,40,41]. In any case, the convection rolls found at strong shaking (i.e., at large values of $\Gamma > 25$) are the granular analog of Rayleigh-Benard convection, and they must be differentiated from the so-called "boundary-driven" convection [5,7,10,15] that appears at milder shaking ($\Gamma \sim 5$).

In this work we carry out experiments in a purely two-dimensional (2D) container that can accommodate only one layer of particles along the depth of the container, and in doing so we uncover the complete sequence of bifurcations in a 2D vibrofluidized bed as well as provide quantitative results about different patterned states. In a quasi-2D setup of a few-particle-diameter depth, such as that employed by Eshuis *et al.* [36] and Ansari and Alam [37,39], it is difficult to obtain quantitative data on (i) the hydrodynamic fields (density, granular temperature, and velocity) as well as on (ii) particle-level quantities (microstructure, distribution function, etc.). Such quantitative measurements are however possible in a pure 2D container that can accommodate a monolayer of particles along its depth as in the experimental work of Eshuis *et al.* [31]. Our primary focus is (i) to quantify the onset of the transition from the bouncing bed to the Leidenfrost state in terms of different control parameters, (ii) to analyze the microstructure in the latter state and related signatures of transition, (iii) to quantify the temporal order (steady or time periodic) of the Leidenfrost state, and finally (iv) to uncover the possible routes to transition of the LS to convection and eventually to a gas. The characteristics and distinguishing features of different states have also been probed with the help of their mean fields, namely, the density and temperature profiles along the vertical direction. It was speculated in Ref. [36] that the collective motion of particles along the depth of the container may be a prerequisite for the onset of convection at strong shaking. On the contrary, we shall demonstrate that (v) the "Rayleigh-Benard-type" granular convection can be realized in experiments in a 2D monolayer system and (vi) the route to transition to a gaseous state occurs via a novel "single-roll" convection. In particular, the coarsening of a pair of convection rolls leading to the genesis of a "single-roll" structure spanning the length of the container and its subsequent transition to a granular gas were not reported in previous experiments.

II. EXPERIMENTAL SETUP AND METHODOLOGY

The experimental setup consists of a quasi-two-dimensional rectangular Plexiglas container with length (L), width (W), and height (H) of 40, 2.2, and 100 mm, respectively, as depicted in Fig. 1(a), which is vibrated along the vertical direction (y) using an electromagnetic shaker. The width (W) of the cell has been chosen such that it fits a monolayer of spherical glass beads along its width, i.e., $W/d \approx 1$; for example, with $d = 2$ mm diameter glass beads, we have $W/d = 1.1$ which

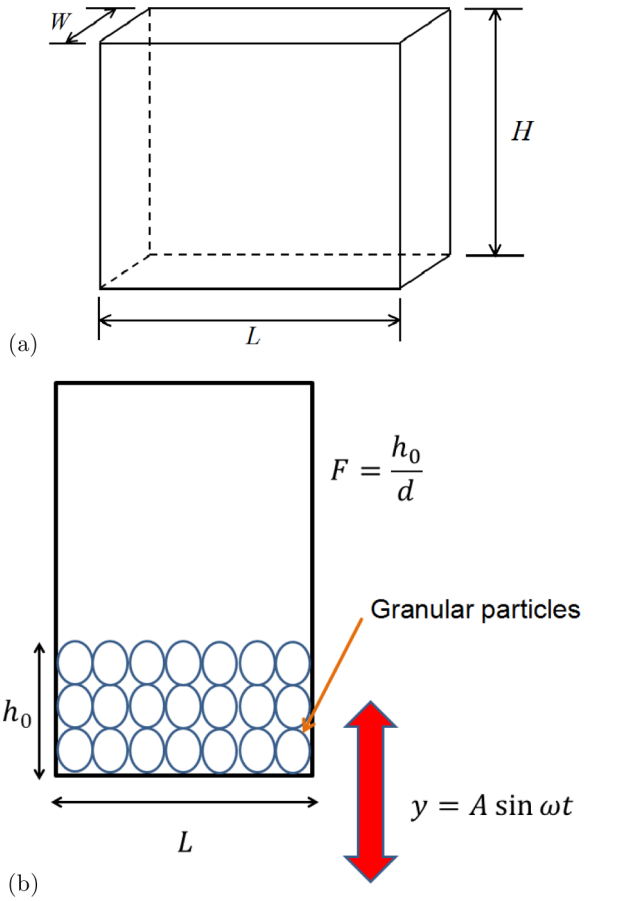

FIG. 1. (a) Schematic of the container with length L, width W, and height H. (b) The container is partially filled with a monolayer (i.e., $W/d \approx 1$) of spherical glass beads of diameter d, and is vibrated harmonically, $y(t) = A \sin \omega t = A \sin 2\pi f t$, via an electromagnetic shaker. $F = h_0/d$ is the number of particle layers at rest.

was kept constant for experiments with even larger diameter particles. A similar Hele-Shaw container was used by Eshuis *et al.* [31] whose work motivated the present work to unveil the complete bifurcation scenario of patterns in a 2D "monolayer" vibrofluidized bed.

A. Experimental protocol and control parameters

The container is partially filled with spherical glass balls (density 2500 kg/m^3) of specified height of $h_0 = Fd$ [where h_0 is the number of particle layers; see Fig. 1(b)]. This particle-filled container is mounted on an electromagnetic shaker (of Ling Dynamics Systems) via a circular head expander [37,39], and is vibrated vertically using a sine wave of the form

$$y = A \sin(\omega t) = A \sin(2\pi f t), \tag{1}$$

where A is the shaking amplitude and f is the frequency of shaking. The shaker operates in a closed loop, controlled by a controller and an amplifier through a software interface. To generate a feedback signal of specified amplitude and frequency of the sinusoidal vibration, a piezoelectric accelerometer is mounted on the head expander.

There are four dimensionless control parameters in this system. The dimensionless shaking acceleration or

intensity,

$$\Gamma = \frac{A\omega^2}{g} = \frac{4\pi^2 A f^2}{g}, \tag{2}$$

is the primary control parameter in this problem. In addition, (ii) the dimensionless shaking amplitude A/d, (iii) the initial layer height,

$$F = \frac{h_0}{d}, \tag{3}$$

where h_0 is the number of particle layers at $t = 0$, and (iv) the length of the container (L/d), which is of crucial importance for the observance of certain patterns (see Sec. III B), constitute the other three control parameters. In this paper, we have restricted ourselves to a relatively narrow container of length $L/d \sim (20,50)$. The last control parameter is the coefficient of restitution (e) for particle collisions; all results are presented for glass beads ($e \approx 0.95$). [Previous works [36] as well as the repetition of a few of the present experiments with steel beads ($e \approx 0.9$) suggest that our reported patterns are robust irrespective of the choice of specific particles.]

Most of the experiments are carried out with $d = 2.0$ mm diameter glass balls; the filling height $F = h_0/d$ is varied from 10 to 50. To check the robustness of reported results, additional monolayer experiments with $d = 5.0$ mm diameter glass balls are also done in a container with $L = 100$, $W = 5.5$, and $H = 100$ mm, respectively, such that $W/d = 1.1$. Once the container is filled with a specified number of layers of particles F, the experiments are conducted at a specified shaking amplitude A/d, but by increasing the shaking frequency f (and hence increasing the shaking acceleration Γ) linearly at a specified sweep or ramping rate. (This type of frequency sweeping at a constant amplitude is achieved by our closed-loop shaker system.) We have used a linear sweep rate of 0.01 Hz/s, unless stated otherwise, and the results are found to be qualitatively similar for a sweep rate of 0.1 Hz/s. To obtain the phase diagram of patterns to span the control parameter space in the $(\Gamma, A/d)$ plane, the experiments are conducted for a range of Γ and A/d. The shaking intensity Γ is varied from 0 to 55, with its upper limit being set by the maximum payload of our shaker; the shaking amplitude A/d is varied from 0.2 to 4.0, with its upper limit being set by the maximum permissible limit ($A = 9$ mm) of our shaker.

The granular particles held in the vibrating container are illuminated with two white LED light sources of power 25 W, positioned at an oblique angle facing towards the container from both sides. Such type of lighting arrangement provided uniform lighting over the region of interest [37,39]. We employed a high-speed camera (IDT MotionPro Y4S3), mostly at a frame rate of 1000 frames per second, to capture the temporal evolution of the collective motion of particles. The series of snapshots are grabbed in on-board camera memory and later on transferred to computer via USB for postprocessing and data analysis.

B. Image analysis for particle tracking

The acquired images of the granular bed have been used to calculate (i) the coarse-grained density and the granular temperature fields (the results are discussed in Sec. III C), (ii) the pair-correlation function (Sec. IV A), and (iii) the oscillations within the Leidenfrost state (Sec. IV B). For all cases, the particles' detection and their position information, frame by frame, are required to be extracted. Once the image analysis is completed, the particle coordinates are fed into a particle-tracking routine to calculate the velocity of each particle in all frames.

A number of particle-tracking routines have been developed by various research groups and are available as open source. In this study, we employed the Particle Detector and Tracker open-source distribution [42], which consists of an ImageJ plugin for particle detection and tracking from digital videos. This plugin implements the feature point detection and tracking algorithm as described in Ref. [43]. It presents an easy-to-use, computationally efficient, two-dimensional, feature point tracking tool for the automated detection and analysis of particle trajectories as recorded by high-speed imaging. The feature point tracking problem consists of detecting images of particles in a digital image sequence and linking these detections over time to follow the tracks of individual particles.

III. PATTERN TRANSITION AND HYDRODYNAMIC FIELDS

A. Transition from bouncing-bed to Leidenfrost state: Phase diagram and scaling

The phase diagram in the $(\Gamma, A/d)$ plane for $F = 25$ layers of 2.0 mm diameter glass beads is displayed in Fig. 2. There are three regimes in Fig. 2: the solid bed (SB), bouncing bed (BB), and Leidenfrost state (LS). At any A/d with $\Gamma \leqslant 1$, the granular bed moves synchronously with the shaker motion

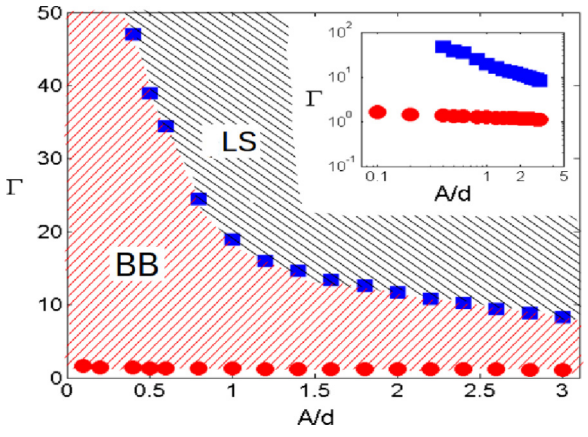

FIG. 2. Phase diagram in the $(\Gamma, A/d)$ plane for $F = 25$ layers of $d = 2.0$ mm diameter glass balls confined in a Hele-Shaw container of width $W/d = 1.1$ and length $L/d = 20$; inset shows the same phase diagram in logarithmic scale. Regions of bouncing bed (BB) and Leidenfrost state (LS) are hatched in the main panel; the region below red circles represents "solid bed" (SB). The symbols represent approximate locations of the respective transition; they are obtained by running experiments at fixed values of A/d by increasing frequency at a linear ramping rate of 0.01 Hz/s; the "up-sweeping" and "down-sweeping" experiments yielded almost the same result for the onset of patterns, suggesting a "supercritical" transition between different states.

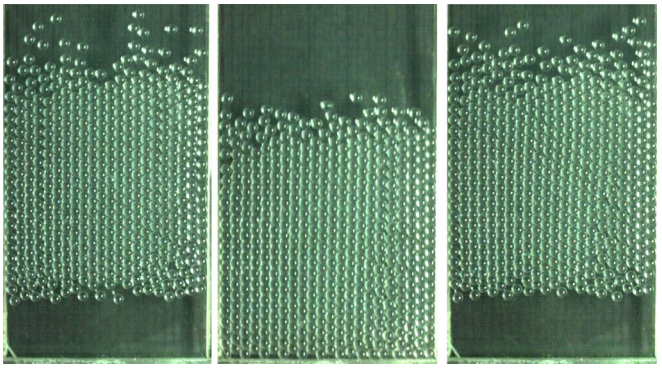

FIG. 3. Snapshots of the bouncing bed (BB) at three successive instants of the oscillation cycle: $t = 0\tau$ (left), $t = \tau/2$ (middle), and $t = \tau$ (right). The shaking acceleration and amplitude are $\Gamma = 5$ ($f = 16.08$ Hz) and $A/d = 2.4$, respectively, with other parameters as in Fig. 2.

without getting detached from the container base; this is the regime of the solid bed (SB). As the shaking intensity is increased beyond some critical value ($\Gamma > 1$), the particles get detached from the base of the container and start a collective motion resembling that of a single particle bouncing off a plate; this is dubbed the bouncing bed (BB) regime. Three successive snapshots of the BB at $t = 0$, $\tau/2$, and τ, where $\tau = 1/f$ is the period of shaking, are displayed in Fig. 3 for parameter values of $\Gamma = 5$ and $A/d = 2.4$. The inset in Fig. 2 indicates that the transition from the solid bed to the bouncing bed regimes occurs at a shaking intensity $\Gamma_{\rm SB}^{\rm BB}$ that remains relatively independent of the shaking amplitude A/d. Note that the data points in Fig. 2 represent boundaries between different states; they have been obtained (i) via a visual inspection of running images on the computer while carrying out experiments and (ii) later via a frame-by-frame analysis of the acquired high-speed images (1000 frames/s); in addition, we have also checked their accuracy by calculating the coarse-grained density and velocity fields (see Sec. III C) at two locations above and below several transition points.

If one increases the shaking intensity (Γ) from the BB regime beyond some critical value (see Fig. 2), the bouncing bed transits to a "density-inverted" state [8,26,31]. The latter corresponds to a state in which a dense region of nearly crystal-packed particles floats over a dilute region of fast moving particles, dubbed the "floating-cluster" [26] or granular "Leidenfrost" state (LS) [31]. The characteristic features of the LS are evident from Fig. 4 which shows three successive snapshots at $t = 0$, $\tau/2$, and τ of the LS over an oscillation cycle at a shaking acceleration of $\Gamma = 30$.

The blue squares in Fig. 2 (see also its inset) indicate that the transition from the bouncing bed to the granular Leidenfrost state depends strongly on the shaking amplitude A/d. The inset on logarithmic scale confirms that the corresponding critical shaking acceleration $\Gamma_{\rm BB}^{\rm LS}$ at which this transition occurs follows a power law:

$$\Gamma_{\rm BB}^{\rm LS} \equiv \Gamma_c \approx 20.74\left(\frac{A}{d}\right)^{-\frac{7}{8}}. \tag{4}$$

At higher shaking amplitudes the onset of LS is expected to occur at lower values of Γ since the input energy

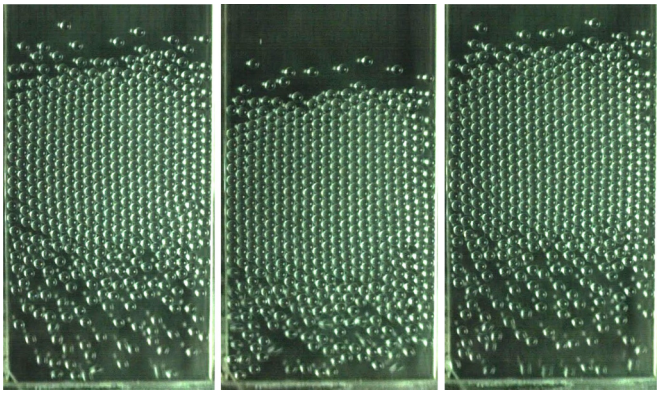

FIG. 4. Snapshots of the granular Leidenfrost state (LS) at three successive time instants of the oscillation cycle: $t = 0$ (left), $t = \tau/2$ (middle), and $t = \tau$ (right). The shaking acceleration is $\Gamma = 30$ ($f = 39.4$ Hz), with other parameters as in Fig. 3.

(via shaker) to the granular materials is proportional to $\Gamma(A/d)$.

Similarly to Fig. 2, we have performed a series of experiments by varying the initial filling height F of 2 mm diameter glass beads as well as by varying the diameter of beads. These data on the critical values of $(\Gamma, A/d)$ for the onset of the Leidenfrost state are displayed in Fig. 5 as denoted by different symbols. It is seen that for a given A/d the critical shaking acceleration for the BB $\rightarrow$ LS transition, $\Gamma_{\rm BB}^{\rm LS}$, increases with increasing F. This dependence on F is expected since increasing F increases the weight of the granular bed which, in turn, requires a higher shaking intensity (Γ) to get transition.

To determine the dependence of $\Gamma_{\rm BB}^{\rm LS}$ on the initial filling height F, we assume that the power-law scaling, Eq. (4), with A/d holds for all F, to be verified *a posteriori*. All data of Fig. 5 are now rescaled via

$$\widetilde{\Gamma} = \Gamma(A/d)^{7/8}, \tag{5}$$

and its variation with F is shown in the upper inset of Fig. 6 on a logarithmic scale. It is clear that $\widetilde{\Gamma}$ has a power-law scaling

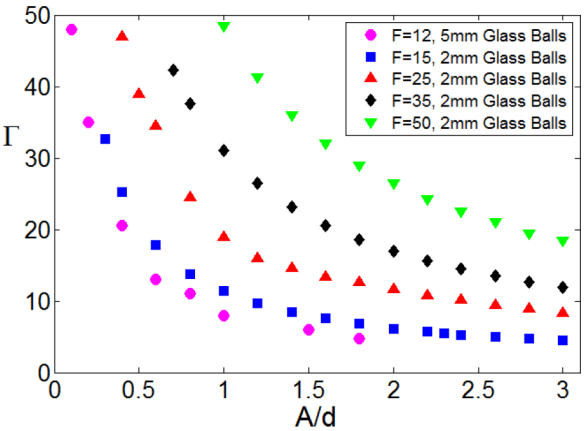

FIG. 5. Effect of filling height $F = h_0/d$ on the BB $\rightarrow$ LS transition; see the legend for F values, with other parameters as in Fig. 2.

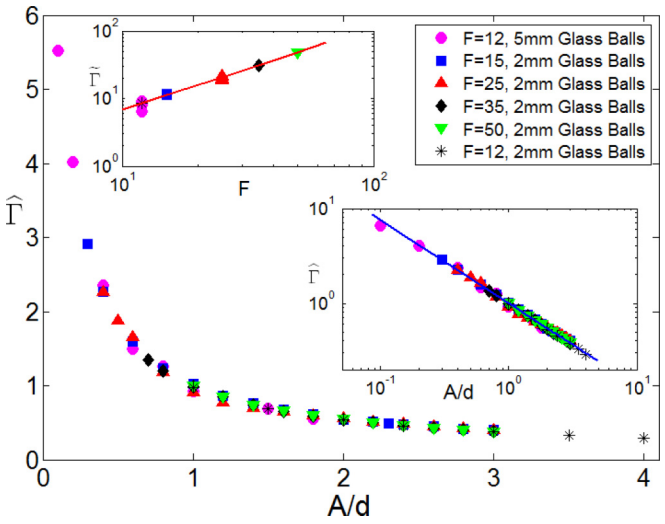

FIG. 6. Master phase diagram in the $(\widehat{\Gamma}, A/d)$ plane, where $\widehat{\Gamma} = \Gamma/\alpha F^{\beta}$. The bottom inset displays the same phase diagram in logarithmic scale, with the blue line representing the power law $\widehat{\Gamma} \sim (A/d)^{-7/8}$. The top inset shows the variation of $\widetilde{\Gamma}$, Eq. (5), with F, with the red line being the best-fit curve. The star symbols refer to the data in Fig. 9 ($L/d = 40$ and $F = 12$).

with F:

$$\widetilde{\Gamma} = \alpha F^{\beta}. \tag{6}$$

The slope and intercept of the best-fit curve (the red line in the upper inset) yield

$$\alpha \approx 0.414, \quad \beta \approx 1.217. \tag{7}$$

To demonstrate that the same power-law dependence on the shaking amplitude [$\sim (A/d)^{-7/8}$, Eq. (4)] holds for all F, we plot the variation of the quantity

$$\widehat{\Gamma} = \frac{\Gamma}{\alpha F^{\beta}} \equiv (A/d)^{-7/8} \tag{8}$$

with A/d in the main panel of Fig. 6. It is seen that all experimental data for different F and d collapse very well on a single curve. The same data are replotted on logarithmic scale in the lower inset of Fig. 6 which reconfirms the universality of the power-law scaling, Eq. (8), of $\widehat{\Gamma}$ with A/d.

In summary, the critical shaking acceleration, $\Gamma_{\rm BB}^{\rm LS}$, for the BB $\rightarrow$ LS transition satisfies the following master equation:

$$\Gamma_{\rm BB}^{\rm LS} \equiv \Gamma_c = 0.414 F^{1.217} \left(\frac{A}{d}\right)^{-\frac{7}{8}}, \tag{9}$$

representing the blue line in the lower inset of Fig. 6. Rewriting Eq. (9) in terms of shaking strength $S = \Gamma \times (A/d)$ (which is the ratio of the average kinetic energy injected to the system via shaking and the potential energy of all particles [31,35]), we obtain

$$S_{\rm BB}^{\rm LS} \equiv \Gamma_{\rm BB}^{\rm LS} \times (A/d) = 0.414 F^{1.217} \left(\frac{A}{d}\right)^{\frac{1}{8}}, \tag{10}$$

which depends on A/d, albeit weakly. In contrast, the previous work of Eshuis *et al.* [31] in a similar setup found the constancy of S at the BB $\rightarrow$ LS transition [their experiments correspond to lower values $A/d \sim O(0.1)$]. This weak increase of S with increasing A/d might be tied to (i) increased frictional barrier at the front and back walls in the same limit and/or (ii) the coupling with the "time-dependent" bottom boundary condition. Ideally, the temperature boundary condition at the vibrating wall should depend on both the shaking amplitude A/d and its frequency f as well as on time; averaging over one oscillation cycle leads to a time-independent constant temperature at the base [31,35,40]. Additional experiments along with theoretical analyses with time-dependent boundary condition are needed to settle the issue of the increase of the critical shaking intensity with increasing A/d, Eq. (10), in a future work.

B. Genesis of convection from Leidenfrost state: Multiroll transition

Now we probe the effect of the length of the container on phase transition and related patterns (SB, BB, and LS) observed in the previous section. The primary motivation of using a larger box is to ascertain whether the monolayer vibrofluidized bed admits convective motion whose origin may then be tied to the instability of the Leidenfrost state. Similar transition has been reported previously [36,37,39], however, in a quasi-2D box (with a depth of a few particle diameters, $W/d \approx 5$) as well as in a 3D box. It was speculated in Ref. [36] that the collective motion of particles along the depth of the container could be a prerequisite for the onset of convection motion at strong shaking.

We used the same glass beads (of diameter $d = 2.0$ mm) in a box of length $L/d = 40$ which is twice that used ($L/d = 20$) in Sec. III A, but other dimensions of the container ($W/d = 1.1$ and $H/d = 100$) remain the same as before. For the sake of demonstration, we present one set of results for a filling height of $F = 12$ layers at a shaking amplitude of $A/d = 4$. The snapshots of patterns with increasing shaking Γ are shown in Figs. 7(a)–7(e). The top row [panel (a)] of Fig. 7 depicts three successive snapshots of the bouncing-bed (BB) state at $\Gamma = 2$, whereas the second row [panel (b)] displays the same temporal sequence of the Leidenfrost state (LS) at $\Gamma = 30$. At a higher shaking intensity of $\Gamma = 40$, the system shows a pair of convection rolls [Fig. 7(c); see also movie 1 in the Supplemental Material [46]). Interestingly, the "2-roll" convection coarsens into a "single roll" at even higher shaking intensity, an example of which is shown in Fig. 7(d) at $\Gamma = 45$ (see movie 2 of the Supplemental Material [46]). There is a dense cluster of particles at one side of the container and a relatively dilute region at the other side; the hotter particles go up from one side, and rain down from the other side, forming a dense cluster. To our knowledge, such "1-roll" convection pattern has not been reported in previous experiments on vibrofluidized beds at strong shaking.

The 1-roll convection persists even at $\Gamma = 50$ (movie 3 of the Supplemental Material [46]), but the cluster on the right side becomes relatively dilute (compared to the case at $\Gamma = 45$). Further increasing Γ leads to extreme agitation of beads, which in turn destroys the convective motion and vaporizes the system into a gaseous state (a granular gas); the snapshots of such a pattern are shown in Fig. 7(e) at $\Gamma = 55$.

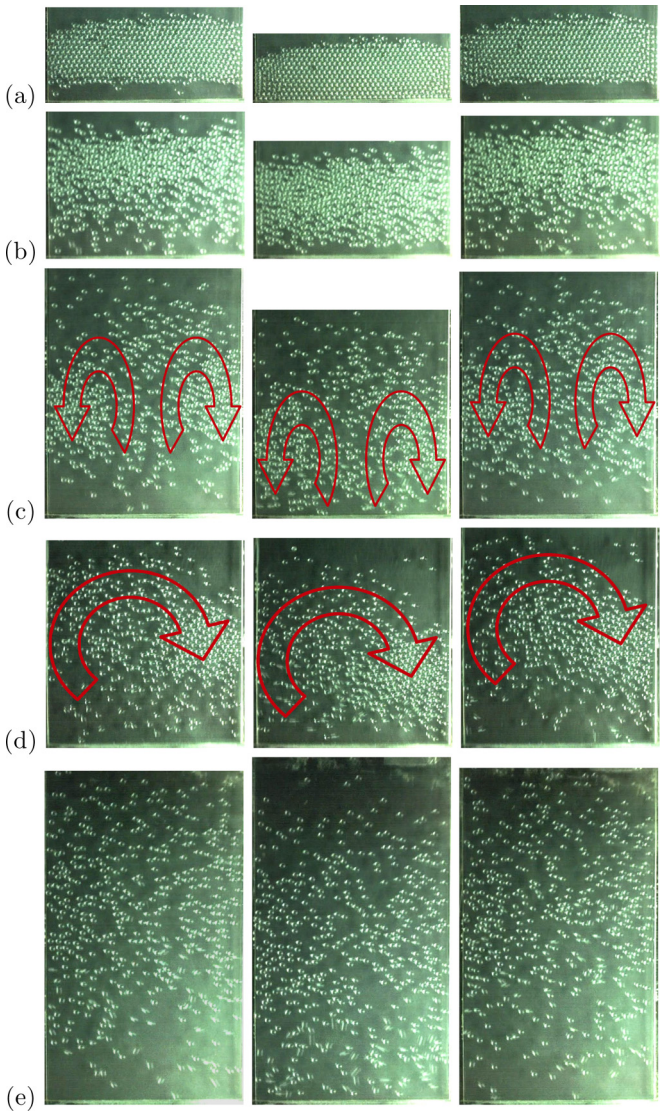

FIG. 7. Three successive snapshots of the bed at $t = 0$ (left), $t = \tau/2$ (middle), and $t = \tau$ (right). (a) Bouncing bed (BB) at $\Gamma = 2$ ($f = 7.8$ Hz); (b) Leidenfrost state (LS) at $\Gamma = 30$ ($f = 30.5$ Hz); (c) convection with a pair of rolls at $\Gamma = 40$ ($f = 35.24$ Hz); (d) convection with a single roll at $\Gamma = 45$ ($f = 37.4$ Hz); (e) gas at $\Gamma = 55$ ($f = 41.3$ Hz). The curly arrows in panels (c) and (d) represent the directional sense of convective motion. The length of the container is $L/d = 40$ and the shaking amplitude is $A/d = 4$ for all cases; other parameters are $F = h_0/d = 12$ and $d = 2.0$ mm diameter glass beads. Movies showing patterns, as in panels (c) and (d), are available as Supplemental Material [46].

The coarse-grained velocity fields of the snapshots of Figs. 7(c) and 7(d) are displayed in Figs. 8(a) and 8(b), respectively. The velocity of the collective motion of particles has been determined by analyzing the acquired images using commercial PIV (particle image velocimetry) software, Dynamic Studio Software, Version 3.3, of Dantec Dynamics A/S, Denmark [44]. For this purpose, the adaptive correlation technique [44,45] was used in which the size of the interrogation window was varied adaptively from 64×64 to 16×16 pixels, with 50% overlap. It is clear from Fig. 8(a) that the PIV velocity field exhibits a pair of convection rolls. Note that this represents an instantaneous velocity field, calculated over two frames separated by 1 ms; however, due to the small number of particles in the system, the accuracy of the calculated velocity field is limited; here we are interested only in the gross features of the hydrodynamic velocity field, i.e., whether it contains a circulating motion or not. Further increasing the shaking intensity to $\Gamma = 45$, the 2-roll convection degenerates into a single roll as is evident from the PIV velocity filed in Fig. 8(b). It is clear that the circulation of this roll is in the clockwise sense; we have confirmed by repeating experiments that the 1-roll convection can also have a counterclockwise circulation for which the dense cluster is formed on the left side of the container.

For a filling height of $F = h_0/d = 12$, we have conducted a series of experiments covering a range of Γ and A/d; various patterns observed and their transitions have been assimilated to construct a phase diagram in the $(\Gamma, A/d)$ plane as shown in Fig. 9. It is seen that the critical shaking intensity corresponding to the onset of LS ($\Gamma_{\rm BB}^{\rm LS}$) follows the same decaying trend with increasing shaking amplitude A/d as reported for the previous set of experiments (refer to the star symbols in Fig. 6). Further increasing Γ, first we find a transition of the LS to the convection motion with a pair of rolls spanning the length of the container, and subsequently to a single-roll convection pattern. It may be noted that the 1-roll convection patterns are observed at $A/d > 2$ and $\Gamma > 42$ and the gaseous state is observed for $A/d \geqslant 3.5$ and $\Gamma > 50$. We reckon that the absence of the LS $\rightarrow$ convection transition in the phase diagram in Fig. 2 can be tied to the fact that a pair of rolls [such as in Fig. 8(a)] cannot be fitted into a container of length $L/d = 20$. In summary, a 2D monolayer vertically vibrated granular system (of sufficient length L) admits Rayleigh-Benard-type convection rolls at strong shaking: the convection sets in from an instability of the LS (beyond a critical shaking intensity), leading to a pair of rolls, which degenerates into a single-roll pattern with increasing Γ and subsequently to a granular gas. The route to the gaseous state from a 2-roll convection to 1-roll convection is a finding of our experiments. A similar transition has been reported in a recent simulation work [47]; see the discussion below.

It is interesting to compare our findings on the LS $\rightarrow$ convection transition in a monolayer system with previous experiments of Eshuis *et al.* [36] in a quasi-2D box of width $W/d = 5.5$ and length $L/d = 100$. Returning to Fig. 9 we find that the critical shaking intensity for the onset of 2-roll convection, $\Gamma_{\rm LS}^{\rm con}$ (denoted by the plus symbols), decreases with increasing shaking amplitude,

$$\Gamma_{\rm LS}^{\rm con} = 42.7(A/d)^{-0.157}, \tag{11}$$

and therefore the related shaking strength,

$$S_{\rm LS}^{\rm con} \equiv \Gamma_{\rm LS}^{\rm con}(A/d) = 42.7(A/d)^{0.843}, \tag{12}$$

increases strongly with increasing shaking amplitude. A careful analysis of the experimental data [36] [compare their data for $A/d = 2$ and 4 in their Fig. 11 for a range of $F \in (4,12)$] reveals that $S_{\rm LS}^{\rm con}$ increases weakly with increasing A/d. The soft-particle molecular dynamics simulations (see Fig. 2 in Ref. [40] and Fig. 9 in Ref. [41]) of the same

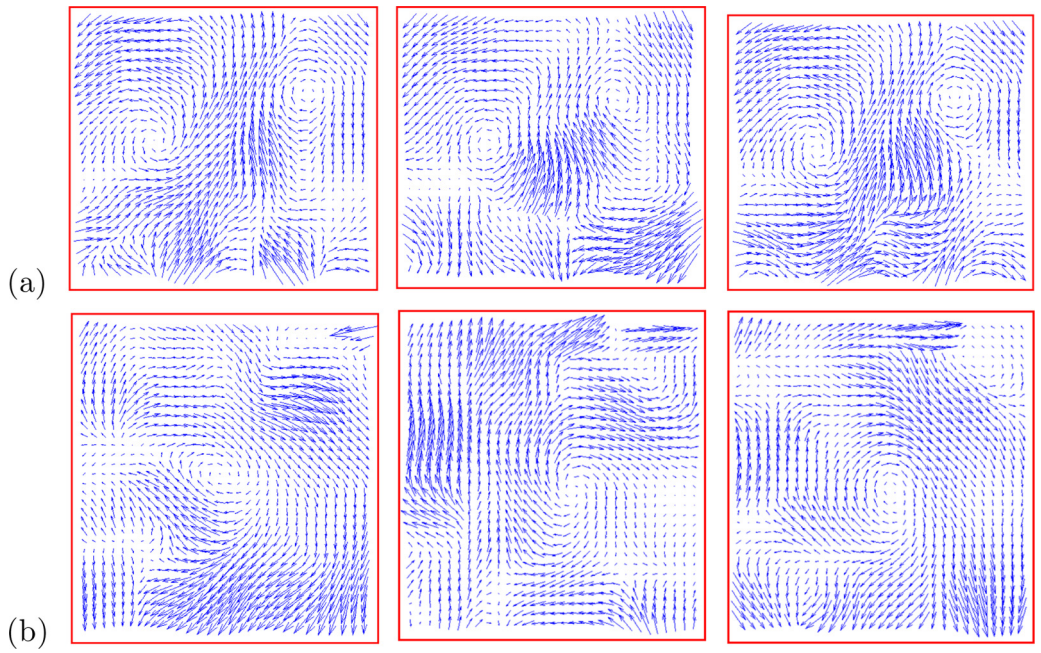

FIG. 8. Coarse-grained PIV velocity fields for convection states. (a) Convection with a pair of rolls at $\Gamma = 40$ and (b) convection with a single roll at $\Gamma = 45$. The left, middle, and right panels correspond to $t = 0\tau$, $t = \tau/2$, and $t = \tau$, respectively. Parameter values for panels (a) and (b) are the same as in Figs. 7(c) and 7(d), respectively.

quasi-2D system seem to support the dependence of $S_{\rm LS}^{\rm con}$ on A/d; on the other hand, the recent event-driven simulations of Rivas *et al.* [47] (in a quasi-2D box as in experiments of Eshuis *et al.* [36]) indicate that $S_{\rm LS}^{\rm con}$ is almost independent of the shaking amplitude if $L/d > 20$ (see their Fig. 3). The differences between our finding, Eq. (12), and the previous quasi-2D experiments [36,41] remain unresolved at present; this calls for additional experiments and simulations.

Let us now discuss our finding of the "2 rolls → 1 roll" transition with increasing Γ: since the length of the container is held fixed ($L/d = 40$) in Fig. 9, the above-found

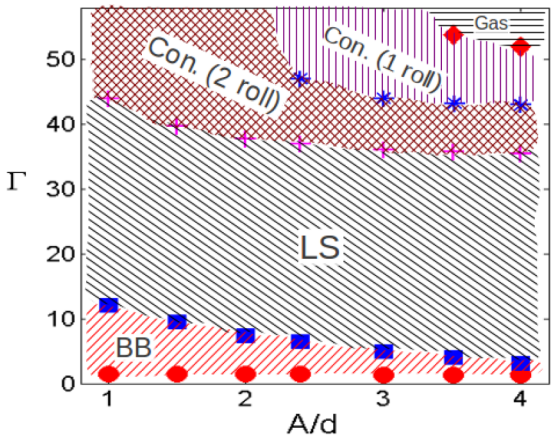

FIG. 9. Phase diagram in $(\Gamma, A/d)$ plane for $F = 12$ layers of 2 mm diameter glass beads confined in $L/d = 40$ cell. Regions of bouncing bed (BB), granular Leidenfrost state (LS), "2-roll" convection, "1-roll" convection, and gas are marked. The symbols represent approximate locations of transition while upsweeping at a specified shaking amplitude A/d with a linear frequency ramping of 0.01 Hz/s.

coarsening of convection rolls is fundamentally different from the appearance of different number of rolls with increasing L/d [36]. Previous quasi-2D experiments (Fig. 12 in [36] and Fig. 4 in [41]) suggest that the convection rolls appear in pairs as the container length L/d is increased when the shaking strength is larger than some minimum value. For given L/d and F, they found that the number of rolls decreases stepwise with increasing S: "the steps involve two rolls at a time, since the pattern always contains an even number of rolls due to the downward motion imposed by the sidewalls" [36]; moreover, their phase diagram (Fig. 14) does not indicate the presence of a gaseous state at larger values of S beyond the convection regime. Interestingly, however, the quasi-2D simulations of Rivas *et al.* [47] found that the above type of coarsening transition with increasing S can occur via a decrease in the number of rolls in step 1 (see their Fig. 2 for $A/d = 4$), depending on the container length L/d, as follows: (i) from "4 rolls → 3 rolls → 2 rolls → gas" for $80 < L/d < 100$, (ii) from "3 rolls → 2 rolls → gas" for $50 < L/d < 80$, (iii) from "2 rolls → gas" for $20 < L/d < 50$, (iv) from "2 rolls → 1 roll → gas" for $15 < L/d < 20$, (v) from "1 roll → gas" for $10 < L/d < 15$, and (vi) "LS → gas" for $L/d < 10$. Our 2D experiments with $L/d = 40$ correspond to case (iii) and hence a "2 rolls → gas" transition is expected which is different from "2 rolls → 1 roll → gas" transition that we found at $A/d = 4$ (see Fig. 9). On the other hand, our experiments with $L/d = 20$ did not show any transition to convection (Figs. 2 and 5) even at $\Gamma = 55$ and $A/d = 4$ (i.e., $S = 220$).

It may be noted that all related simulations [40,41,47] have been done in a quasi-2D box, closely following the experimental setup of Eshuis *et al.* [36], and, moreover, the driving in Ref. [47] is *bi-parabolic* [rather than via the sine function as in Eq. (1)]. The recent simulations [47]

predicted a transition route of "4 rolls → 3 rolls → 2 rolls → gas" [the case (i) above, with increasing Γ] for a container of length $L/d = 100$ which may be contrasted with the previous experimental finding [36] of "6 rolls → 4 rolls → 2 rolls" convection, indicating an anomaly in the simulated predictions on the number of rolls in the same setup having similar parameter values. In addition, our recent experiments [35] in a quasi-2D box ($W/d = 5.5$) with $L/d = 80$ found that the primary bifurcation from the Leidenfrost state is a 4-roll convection pattern in contrast to the 3-roll pattern observed in simulations [47].

Overall, the above comparative discussion suggests that, to make a one-to-one comparison with our experimental findings on the "multiroll" transition scenario (via "2 rolls → 1 roll → gas" with increasing Γ at $L/d = 80$), future simulations should be carried out in a monolayer box under harmonic shaking with parameter values as in the present experiments. We also recommend additional experiments by increasing the length of the container L/d to see whether the multiroll transition scenario as depicted in Fig. 2 of Ref. [47] survives in a two-dimensional vibrofluidized bed.

C. Density, granular temperature, and temperature anisotropy

To assess the structure of the shaken granular bed with varying Γ and A/d, we measured the coarse-grained density and temperature profiles from image analysis using the ImageJ software as described in Sec. II B. The density profiles along the vertical direction have been calculated from the digitized (binary) version of the experimental snapshots by determining an "effective" normalized pixel density (i.e., by counting pixels that constitute the beads) over a box of height 5 pixels and width equal to the image width in pixels. The density profile is subsequently smoothed by fitting the data via a polynomial.

The "granular" temperature is defined as the mean square of the velocity fluctuations around the mean flow velocity:

$$T = \tfrac{1}{2} m \langle (\mathbf{v} - \mathbf{u})^2 \rangle, \tag{13}$$

where $\mathbf{v}$ is the instantaneous particle velocity and $\mathbf{u} = \langle \mathbf{v} \rangle$ is the hydrodynamic or flow velocity (which vanishes in the present case of a harmonically shaken bed) and the angular bracket denotes a suitable averaging over many snapshots of the system. Once the individual particle position is extracted for a batch of snapshots using the particle-tracking routines, the individual particle velocity can be determined from two successive frames, which are fed into Eq. (13) to obtain the temperature field. More specifically, the granular temperature at a specified height, $T(y)$, is calculated by dividing the system into a series of horizontal bins or layers of height of 2 particle diameters and width as that of snapshot (assuming horizontal homogeneity). In each bin (say, at $y = y_i$), the averaging is carried out (i) over all particles inside the bin in each snapshot as well as (ii) over a batch of 400 snapshots or more that span over many oscillation cycles.

Figure 10(a) displays the density profiles with increasing shaking intensity Γ at a shaking amplitude of $A/d = 2.4$ (see Fig. 2). The density profile in the BB state observed at $\Gamma = 5$ is indicated by the red curve in Fig. 10(a); the corresponding snapshots of the system are shown in Fig. 3. The density shows a slight increase from the base of the container to a

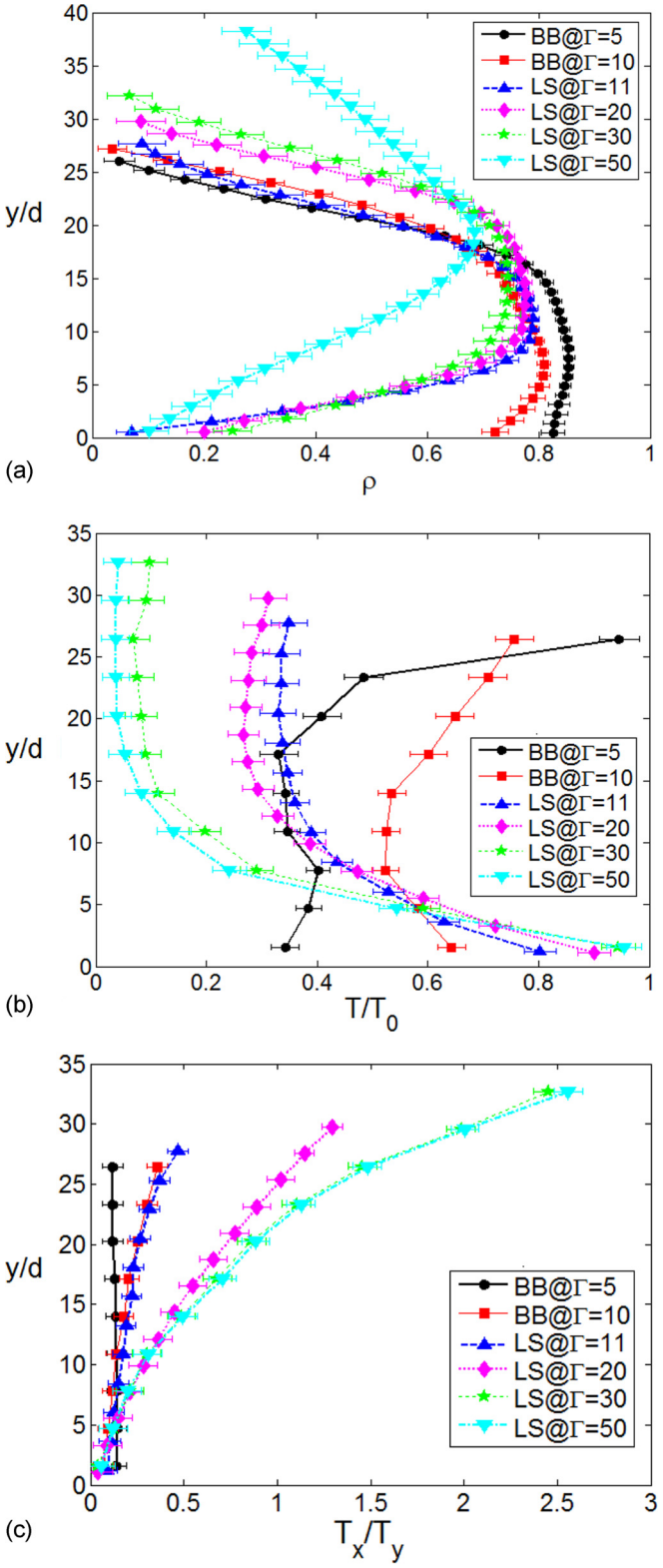

FIG. 10. Variations of (a) density and (b) granular temperature with height for the various states in $F = 25$ layers of 2.0 mm diameter glass beads at constant $A/d = 2.4$ with increasing shaking intensity Γ. Here, T_0 is the input shaking energy (per particle) at the base. (c) Profiles of the temperature ratio T_x/T_y such that $T = (T_x + T_y)/2$; note that the data for $\Gamma = 30$ and 50 almost overlap with each other.

height corresponding to the maximum density, beyond which it remains nearly constant over a certain height, representing a region wherein the particles are packed hexagonally (see the snapshots in Fig. 3). Beyond a certain height the density shows a rapid fall indicating the existence of a dilute gas-like layer of fast moving particles on the top of the bed. It is noteworthy that the density profile of the BB state at a higher shaking intensity $\Gamma = 10$ (just below the transition to LS; see Fig. 2) shows a weak "density inversion." Furthermore, the maximum density which the bed has achieved is slightly smaller than the maximum density attained at $\Gamma = 5$; this is expected since the bed at higher Γ is likely be loosely packed due to the relatively higher degree of fluidization. The density profile of BB at $\Gamma = 10$ [see the red curve in Fig. 10(a)] follows almost the same trend of the density decay as that of BB at $\Gamma = 5$ beyond the maximal density height. It is also noticeable that the density profile at higher Γ spans a larger height due to the higher input shaking energy (due to which the particles on the top of the bed bounce off to a greater height).

Increasing the shaking intensity from $\Gamma = 10$ to $\Gamma = 11$, an extreme *density inversion* [see the blue curve in Fig. 10(a)] is found to occur. This signals that the system has transited to the Leidenfrost state (LS) in which a dense cluster floats over a dilute gaseous layer and the maximum density within the floating cluster is much lower than that in the bouncing bed (at $\Gamma = 10$). Further increasing Γ leads to an overall expansion of the granular bed in which the extent of the floating cluster gradually reduces and the dilute gaseous region beneath grows in size. Comparing the green ($\Gamma = 30$) and light blue ($\Gamma = 50$) curves in Fig. 10(a), we find that the density reduction above the floating cluster becomes more gradual with increasing Γ, implying that there exists a "saltating" layer of particles above the dense cluster where the particles move ballistically; this is dubbed the *ballistic layer*.

To summarize Fig. 10(a), we found that the granular Leidenfrost state is characterized by three distinct regions: (i) a dense *floating cluster*, (ii) a dilute gaseous *collisional layer* adjacent to the base of vibrating container, and (iii) a *ballistic layer* consisting of fluidized particles on the top of the floating cluster. Note that the ballistic layer is also present in the BB state above the crystal-packed layer (see the snapshots in Fig. 3).

Corresponding to the density profiles in Fig. 10(a), the profiles of granular temperature $T(y)$ and the temperature ratio $[T_x/T_y$, where T_i is the temperature along the ith direction such that $T = (T_x + T_y)/2]$ are shown in Fig. 10(b) and Fig. 10(c), respectively. The temperature has been normalized by the average input energy T_0 at the base. In the case of BB states at $\Gamma = 5$ and 10, the temperature remains nearly constant up to the height of the "crystalline" packed bed, but increases at higher elevations due to the higher kinetic energy possessed by the fluidized particles at the top. In the case of LS, however, the temperature monotonically decreases from the vibrating base up to the top of the floating cluster. This confirms that a dense cluster of particles floats over fast-moving/hotter particles in the granular Leidenfrost state. Comparing the temperature profiles between BB and LS in Fig. 10(b), we find that the granular temperature in BB states is lower near the vibrating base in contrast to the LS for which maximum temperature occurs at the base; this is a distinguishing criterion between BB and LS. The origin of the comparatively higher temperature near the base in the LS can be tied to the hotter dilute region which is absent in the BB state.

Figure 10(c) indicates that the temperature ratio in the BB at $\Gamma = 5$ is small and remains almost constant ($T_x/T_y \approx 0.15$); however, at $\Gamma = 10$, this ratio increases with elevation from the base. The latter observation also holds in the case of LS at $\Gamma = 11$ and higher Γ. Overall, the temperature in the vertical direction is larger than that in the horizontal direction ($T_y > T_x$, which is expected since the energy is imparted to particles via shaking along the vertical direction) except at very high values of Γ where $T_x > T_y$ near the top of the bed that constitutes the ballistic layer. The latter finding is intriguing since it implies that the vertical component of the temperature can be lower than its horizontal component in the ballistic layer of the vibrofluidized bed. It is conceivable that at large enough Γ the particles in the ballistic layer can loose their momentum in the vertical direction much more easily due to collisions with the floating cluster; on the other hand, their collisions along the horizontal direction are less likely due to the dilute nature of the ballistic region, resulting in higher values of T_x and consequently $T_x/T_y > 1$ in the ballistic region.

The above-discussed characteristic features of the density, granular temperature, and temperature-ratio profiles hold even if we traverse the phase diagram in Fig. 2 at a constant shaking intensity Γ while increasing the shaking amplitude A/d; see Figs. 11(a)–11(c) at $\Gamma = 50$ for various values of A/d spanning both BB and LS. Increasing the shaking amplitude (A/d) beyond a critical value causes a density inversion [see Fig. 11(a)], marking the onset of LS in the system. The maximum density occurs at a certain height away from the base once it crosses the dilute collisional layer and the density remains nearly constant at the maximal value up to a certain thickness spanning the floating cluster, and subsequently drops rapidly across the rarefied ballistic layer at the top of the bed. Other features of the density profile with increasing A/d are similar to those found for increasing Γ as in Fig. 10(a). Figure 11(b) indicates that the temperature in the BB states increases monotonically from the base to the top which is different from the nonmonotonic temperature profiles found in the BB states in Fig. 10(b) for the case of increasing shaking frequency f at constant shaking amplitude. On the contrary, in the LS, the temperature shows a decaying behavior away from the base, attaining a minimum value at the end of the collisional layer, and then increases, albeit mildly, at higher elevations. The degree of increase of $T(y)$ at higher elevations, however, decreases with increasing A/d (compare the T profiles at $A/d = 0.5$ and 1) and the temperature remains almost constant near the top of the bed at $A/d = 2.4$. The latter observations are also evident in Fig. 10(b); see the T profiles at $\Gamma = 20$, 30, and 50. The temperature-ratio (T_x/T_y) profiles in Fig. 11(c) show similar characteristic features as those presented in Fig. 10(c).

It may be noted that the density profiles were first measured in a 2D vibrofluidized bed by Warr *et al.* [12], and some of their density profiles did show signatures of a density inversion [see their Figs. 2(a) and 2(b)]. The overall shapes of our density and granular temperature profiles [Figs. 10(a) and 10(b)] with increasing Γ are found to be similar to those in the 2D simulation of Yang and Hsiau [20] (see their Figs. 5

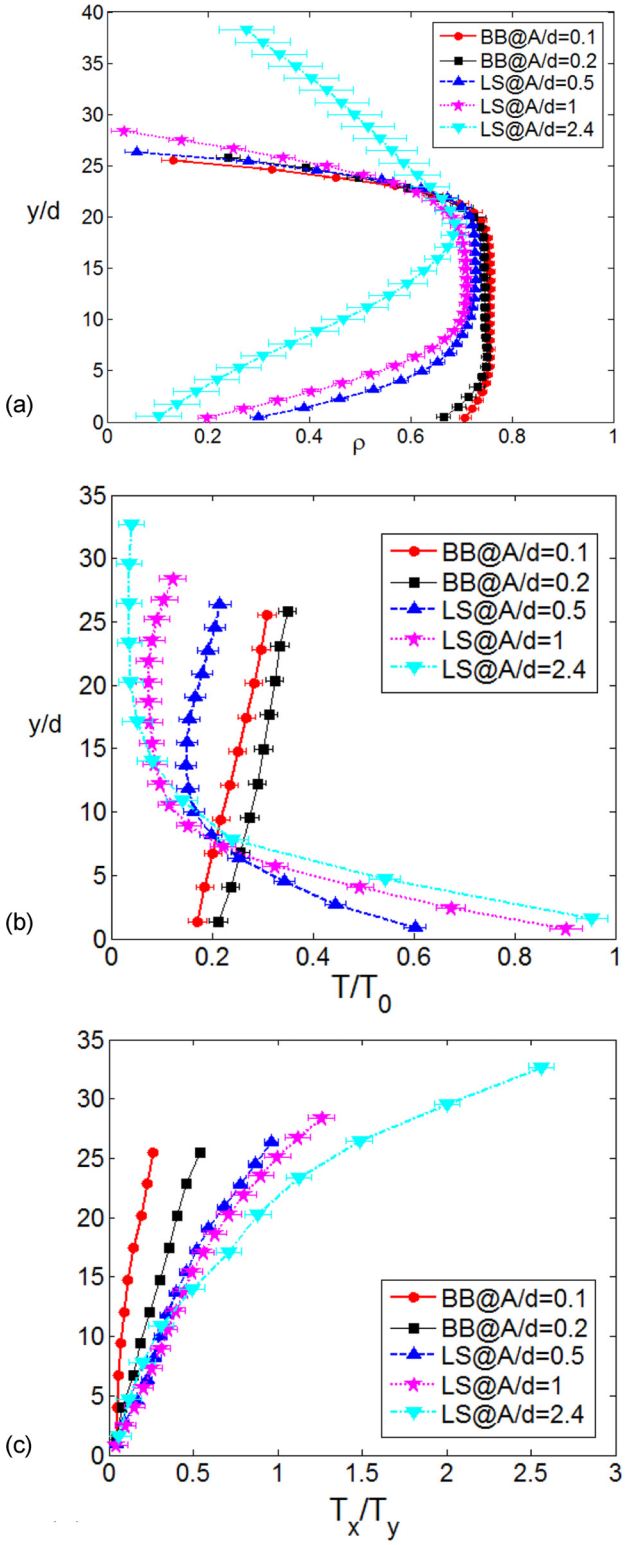

FIG. 11. Same as Fig. 10 but with increasing shaking amplitude A/d at a constant shaking intensity $\Gamma = 50$.

and 6); in particular, the increase of granular temperature at higher elevations in the BB state looks strikingly similar to that in Fig. 6 of Ref. [20]. The related NMR experiments by Huan *et al.* [29] in a 3D vibrofluidized bed identified similar nonmonotonic variations of density and temperature with height. The latter experiments also measured the height profiles of horizontal (T_x) and vertical (T_y) temperatures (see their Figs. 12 and 13), but they always found $T_x < T_y$ for all case studies with $T_x/T_y \approx$ constant with elevation.

IV. MICROSTRUCTURE AND DYNAMICS IN GRANULAR LEIDENFROST STATE

A. Microstructure and spatial-ordering of particles

An important quantity employed for studying the microstructural characteristics and the spatial order of a particulate system is the so-called pair correlation function which describes how, on average, the particles are radially packed around each other. Mathematically, the pair-correlation function is given by [48]

$$g(r) = \frac{1}{N\rho(r)} \sum_{i=1}^{N} \sum_{j \neq i}^{N} \langle \delta(r + r_j - r_i) \rangle, \tag{14}$$

where $\rho(r)g(r)$ is the conditional probability of finding a particle at a distance r away from the reference particle such that

$$\int \rho(r)g(r)dr = N - 1. \tag{15}$$

Since the hydrodynamic fields are inhomogeneous along the vertical direction, first we calculated the one-dimensional pair-correlation function $g(x) = g(x|y_i)$ in a horizontal stripe which is located at $y = y_i$. In the granular Leidenfrost state, the particles belonging to three regions [(i) collisional layer, (ii) floating cluster, and (iii) ballistic layer] are considered separately; we then evaluate $g(x) = g(x|y_i)$ at the center of each region ($y = y_i$) over a horizontal stripe of thickness $\delta y = 1.5d$.

Figures 12(a) and 12(b) display the pair-correlation function $g(x|y_i)$ in three regions of the LS at $\Gamma = 30$ and 50, respectively; other parameters are as in Fig. 10. In both cases, the $g(x)$ in the floating cluster contain an array of peaks: the first peak is located at the contact point, the second peak at $r/d \approx \sqrt{3}$, and other subsequent peaks occurring at regular spacings, signifying a nearly hexagonal-packed structure. The $g(x)$ in the collisional and ballistic regions of the LS indicate that both are gaseous in nature: there is a peak at $r = d$ and then it decays rapidly with distance until it asymptotes to unity at $r/d \approx 2$, suggesting that particles are uncorrelated at large distances. Comparing the $g(x)$ between the ballistic and collisional regions of the LS in Fig. 12, we find that the first peak of $g(x)$ in the ballistic layer is larger than that in the collisional layer. This suggests that the center of the ballistic region [i.e., $y = y_i$ at which $g(x|y_i)$ is calculated] is comparatively denser than that of the collisional region.

With increasing shaking intensity Γ, the collisional and ballistic layers of LS expand and become relatively dilute due to the higher degree of fluidization; consequently there is a decrease in the contact value of $g(x)$ as seen in the respective red and black curves in Figs. 12(a) and 12(b). In a similar manner, the packing within the floating cluster also becomes more and more loose with increasing Γ, causing a minor

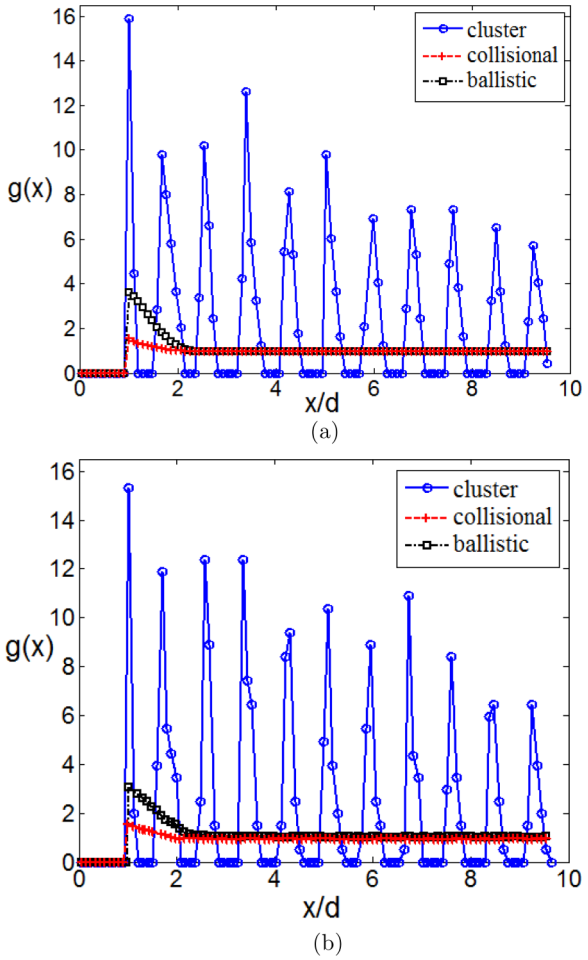

FIG. 12. One-dimensional pair-correlation function, $g(x|y_i)$, in three regions of the Leidenfrost state (LS) at (a) $\Gamma = 30$ and (b) $\Gamma = 50$, with other parameters being $A/d = 2.4$, $F = h_0/d = 25$, and $d = 2.0$ mm. Note that $g(x|y_i)$ is evaluated in a horizontal stripe (of thickness $\delta y = 1.5d$) whose vertical location, $y = y_i$, is approximately at the center of each region. In each panel, the open blue circles refer to the floating cluster, the lower curve marked by red plus symbols refers to the collisional layer, and the middle curve marked by black squares refers to the ballistic layer.

drop in the contact value of $g(x)$; compare the blue curves in Figs. 12(a) and 12(b).

For a better understanding of the orientational ordering of particles in the (x,y) plane, we probed the two-dimensional pair-correlation function $g(r,\theta)$ by mapping $g(r)$ onto polar coordinates (r,θ). The radial-angular correlation distribution $g(r,\theta)$ is defined as [48,49]

$$g(r,\theta) = \frac{1}{N\rho(r,\theta)} \sum_{i=1}^{N} \sum_{j\neq i}^{N} \langle \delta(r - r_{ij}) \delta(\theta - \theta_{ij}) \rangle, \qquad (16)$$

which gives correlations for the pair of particles i and j, the distance between whose centers of mass is r_{ij} and the angle between the plane containing particles i, j and the horizontal plane is θ_{ij}; $\rho(r,\theta)g(r,\theta)$ is the conditional probability of finding a particle at a distance r from a reference particle and in a plane containing a reference particle which makes an angle θ with respect to the horizontal plane. The contour plot of the $g(r,\theta)$ in the (r,θ) plane is likely to reveal the "contact network" of particles in the granular bed, indicating the most probable spatial configuration of particles around a reference particle.

To calculate $g(r,\theta)$, in addition to binning the particles in the radial direction, we also binned them in the angular direction; the number of bins considered in the radial and angular directions are 100 and 20, respectively. Let us first probe the $g(r,\theta)$ in the bouncing-bed state. The contour plots of $g(r,\theta)$ for different shaking amplitude A/d are shown in Figs. 13(a)–13(c); the shaking acceleration is set to $\Gamma = 5$ such that the system is in the BB state (see Fig. 2). The sixfold symmetry of the contact network, resembling the hexagonally packed crystalline structure of the bouncing bed, is clearly evident in Fig. 13(a). With increasing shaking amplitude (A/d), the lattice points of the hexagonal-packing structure get perturbed, thereby breaking the "exact" directional symmetry as it is evident in Figs. 13(b) and 13(c). This is because, as A/d increases, the particles get more loosely packed making them more mobile to move around each other and thus destroying the angular anisotropy of their positions.

The $g(r,\theta)$ in three regions of the LS, namely, the collisional layer, floating cluster, and ballistic layer, are presented in Fig. 14. The reference particle considered in these polar plots is located at the center of the circle. The $g(r,\theta)$ in Fig. 14(a) indicates that the floating cluster is highly anisotropic in nature, showing directional dependence with increased probability of "head-on" collisions (i.e., $\theta = \pi/2, 3\pi/2$). On the contrary, the collisional and ballistic layers in Figs. 14(b) and 14(c), respectively, show angular isotropy which implies that the particles are more likely to be found at any angular orientation on average; this is expected since these regions are in a gaseous phase. A closer look at Fig. 14(a) reveals that the sixfold symmetry of the contact network still survives in the LS, but the hexagonal lattice structure seem to have been significantly modified, with more collisions likely to occur at $\theta = 2\pi/3$ and $4\pi/3$ in addition to head-on collisions. This indicates that the packing of particles in the LS is much looser than the "ideal" hexagonal packing. The latter observation can be further rationalized if we analyze the radial component of the $g(r,\theta)$ [of Figs. 14(a)–14(c)] which is displayed in Fig. 14(d). Note that $g(r) \equiv \langle g(r,\theta) \rangle_\theta$, and hence it provides information on the radial configuration of particles around a test particle over a circular region of diameter equal to the height of the floating cluster. The $g(r)$ in the floating-cluster region [the blue curve in Fig. 14(d)] resembles more a liquid-like structure, with its second peak being located at $r/d \approx 1.9$. Therefore the floating-cluster region is in a liquid state, which hovers over a gas-like collisional layer underneath, and this makes the connection with the original Leidenfrost state [31,38] more appropriate.

B. Height oscillations in granular Leidenfrost state

A closer look at the snapshots (of the Leidenfrost state) in Fig. 4 reveals that the top surface of the granular bed as well as the interface separating the dense floating cluster and the dilute collisional layer do vary with time within an oscillation cycle of the external driving. It is interesting to find out whether there is a definite frequency associated with such height oscillations in the granular Leidenfrost state. To this end, we have tracked

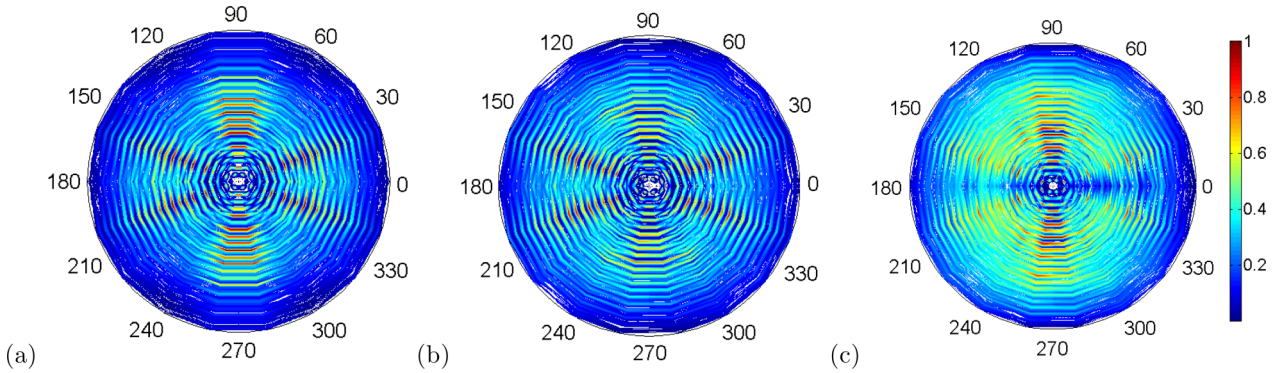

FIG. 13. The radial-angular distribution function $g(r,\theta)$ in the "bouncing bed" state at a shaking acceleration $\Gamma = 5$ with increasing shaking amplitudes: (a) $A/d = 0.5$, (b) $A/d = 1$, and (c) $A/d = 2.4$. Other parameters are as in Fig. 12.

the temporal evolution of two characteristic heights: (i) the location of the top surface of the floating-cluster region $y_{\rm clus}(t)$, and (ii) the height of the collisional layer $y_{\rm coll}(t)$ (i.e., the vertical location of the interface between the floating cluster and the collisional layer beneath), with both being measured from the base of the container; see the sketch in the inset of Fig. 15. The high-speed images of the bed were analyzed to measure $y_{\rm coll}(t)$ and $y_{\rm clus}(t)$ at various time instants over a few shaking cycles. The unsteadiness of the LS, if any, is likely to be implicated in the temporal variations of $y_{\rm coll}(t)$ and $y_{\rm clus}(t)$ as we demonstrate below.

Let us consider the case of LS observed in experiments with $F = 25$ layers of $d = 2$ mm diameter glass beads at a shaking intensity of $\Gamma = 30$ with $A/d = 1.6$ ($f = 48.26$ Hz). The time evolutions of $y_{\rm coll}(t)$ and $y_{\rm clus}(t)$ are shown in Fig. 15; the time has been scaled by time period of driving ($\tau_d = 1/f \approx 20.72$ ms). The experimental data (denoted by red circles) for both $y_{\rm coll}$ and $y_{\rm clus}$ are best fitted by sinusoids (the blue curves in

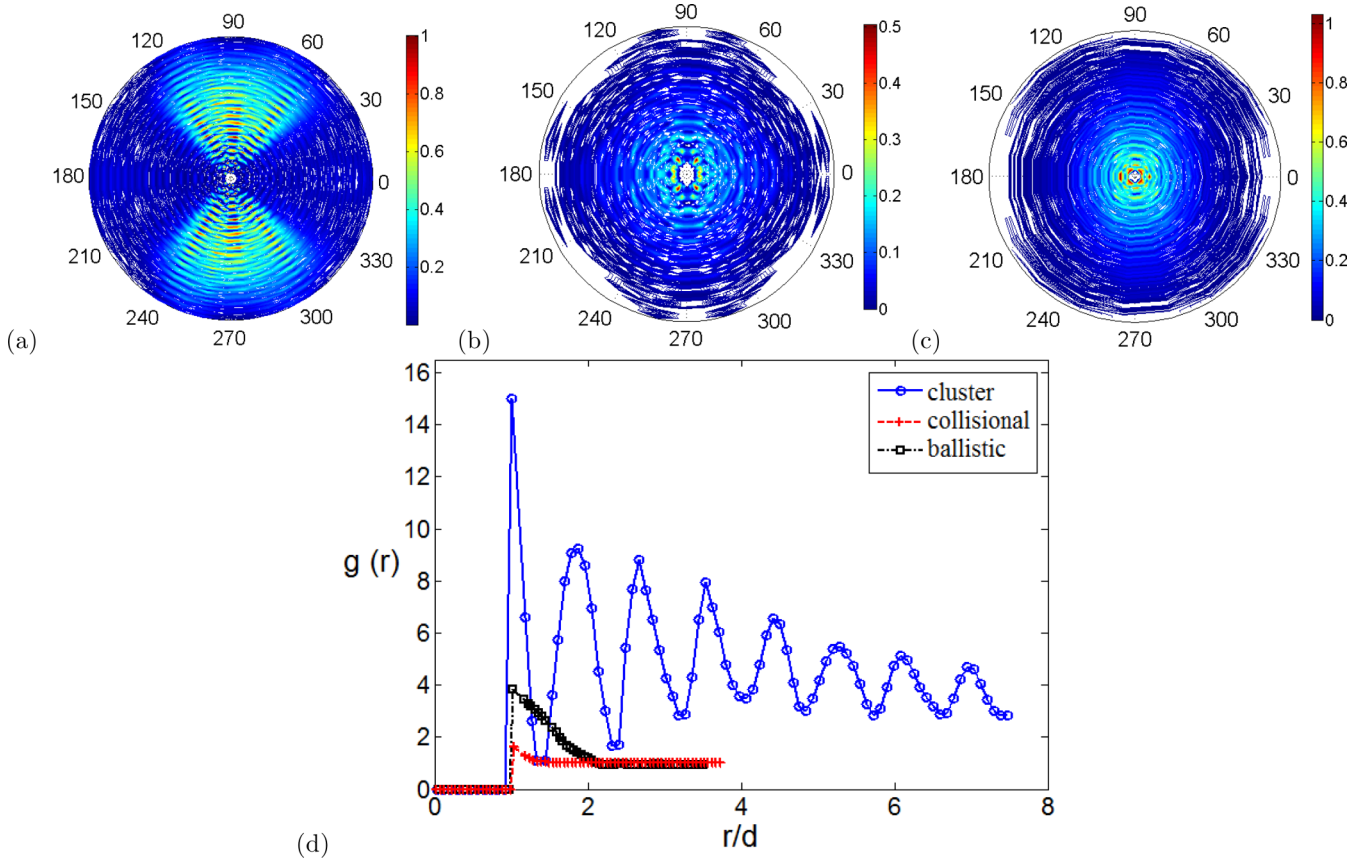

FIG. 14. The radial-angular correlation function $g(r,\theta)$ in various regions of LS: (a) floating cluster, (b) collisional layer, and (c) ballistic layer; other parameters are the same as in Fig. 12. (d) The radial component of the $g(r,\theta)$ in the floating cluster (blue circles), collisional layer (the lower curve marked by red plus), and ballistic layer (the middle curve marked by black squares).

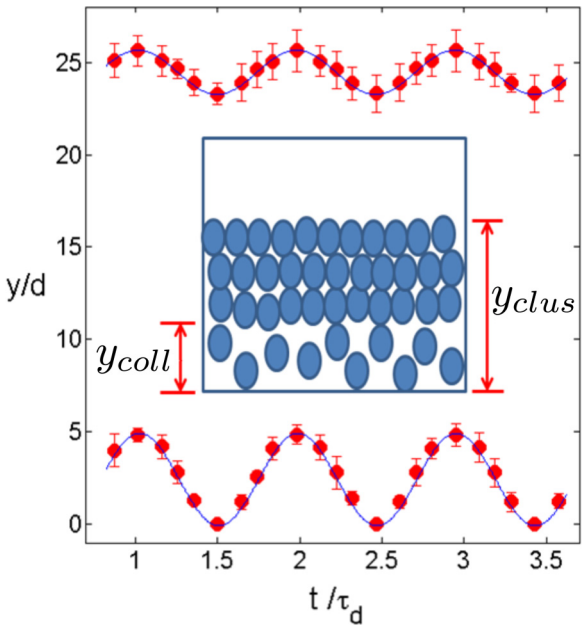

FIG. 15. Temporal variations of $y_{\rm coll}(t)$ and $y_{\rm clus(}t{\rm)}$ at $\Gamma = 30$ and $A/d = 1.6$, with other parameters being $F = h_0/d = 25$ and $d = 2$ mm diameter glass beads. The red circles represent experimental data (with error bar) and the best-fitted curve is denoted by the blue line. Inset depicts a sketch of the Leidenfrost state (LS): $y_{\rm coll}(t)$ is the instantaneous height of the collisional layer and $y_{\rm clus}(t)$ is the vertical location of the top of the floating cluster.

Fig. 15) of the following form:

$$y_{\rm coll}(t)/d = 2.5 + 2.4\sin(0.305t + 1.159), \quad (17)$$

$$y_{\rm clus}(t)/d = 24.46 + 1.2\sin(0.307t + 1.231), \quad (18)$$

where t is the time measured in ms. Note that the oscillation amplitude of the top surface ($\langle y_{\rm clus}(t)\rangle$) is smaller than that of the interface ($\langle y_{\rm coll}(t)\rangle$). From the above equations, the angular frequencies $\omega_{\rm coll}$ and $\omega_{\rm clus}$ are 305 rad/s and 307 rad/s, respectively, which closely agree with the driving angular frequency ($\omega_d = 2\pi f = 303$). Thus, the interface and top surface of the LS oscillates harmonically and is synchronized with the frequency of the external vibration.

To check the robustness of above finding, we analyzed the images of the LS observed in a second set of experiments with 5 mm diameter beads. The temporal variations of $y_{\rm coll}(t)$ and $y_{\rm clus}(t)$ at $\Gamma = 30$ and 43.4 are shown in Figs. 16(a) and 16(b), respectively; other parameters are $A/d = 0.6$ and $F = h_0/d = 12$ (refer to the phase diagram in Fig. 5). While the experimental data for $\Gamma = 30$ are best fitted via the sinusoids of the form

$$y_{\rm coll}(t)/d = 2.2 + 1.84\sin(0.315t + 0.62), \quad (19)$$

$$y_{\rm clus}(t)/d = 15.7 + 0.66\sin(0.31t + 0.864), \quad (20)$$

the data for $\Gamma = 43.4$ are best fitted by

$$y_{\rm coll}(t)/d = 2.7 + 2.53\sin(0.37t - 0.322), \quad (21)$$

$$y_{\rm clus}(t)/d = 16.8 + 0.616\sin(0.377t + 0.118), \quad (22)$$

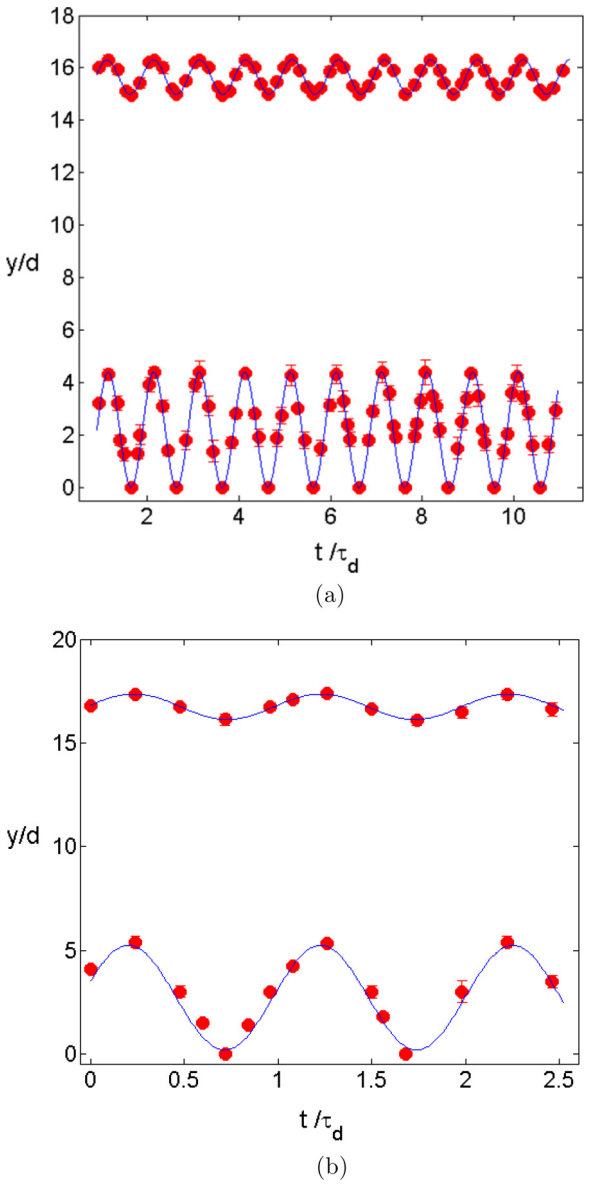

FIG. 16. Same as Fig. 15, but for $F = 12$ layers of $d = 5$ mm diameter glass beads with $A/d = 0.6$: (a) $\Gamma = 30$ and (b) $\Gamma = 43.4$.

where the time is measured in ms. At $\Gamma = 30$, we found that $\omega_{\rm coll} \approx 314.7$ rad/s and $\omega_{\rm clus} \approx 310$ rad/s, which are very close to the driving frequency $\omega_d = 313$ rad/s. At $\Gamma = 43.4$, $\omega_{\rm coll} = 370$ rad/s and $\omega_{\rm clus} = 377$ rad/s, and $\omega_d = 376$ rad/s $\approx \omega_{\rm coll} \approx \omega_{\rm clus}$. Another noteworthy feature in Fig. 16(a) is the absence of low-frequency modulation (even over 12 oscillation cycles) in both $y_{\rm coll}(t)$ and $y_{\rm clus}(t)$.

Collectively, the above analysis indicates that both the interface between the collisional layer and the floating cluster and the top surface of the floating cluster oscillate harmonically and are synchronized with the frequency of the external vibration. Therefore, the granular Leidenfrost state is a *period-1* wave (i.e., an *f-wave*) as is the case for the bouncing-bed.

Although the "synchronous" height oscillations of the LS were never quantified previously, there are simulation works in the same direction. The most recent simulation [47] identified a low-frequency (semiperiodic) oscillation in the

density-inverted state (in a quasi-3D setup of a narrow column of length and width $L/d = 5 - W/d$). They also found delta-like peaks at the driving frequency and its harmonics in the power spectra of the temporal variation of the center of mass of the system [see their Fig. 4(b)]; while the former may be connected to the f-wave nature of the LS as found in our work, the implications of the peaks at the harmonics of f remain unclear. On the other hand, the simulation work of Bougie *et al.* [50] probed the time dependence and density inversion in a vertically vibrated 3D box filled with shallow layers ($F = h_0/d = 4.3$) of granular materials. While they found that the density-inverted state is indeed an f wave in the low-Γ regime ($\Gamma = 5.68$), the density profiles become time invariant in the high-Γ regime ($\Gamma = 56.5$). The latter observation is in stark contrast to our finding in Fig. 16 that increasing Γ from 30 to 43.4 does not seem to have an effect on the f-wave nature of the LS. (It may be noted that the low- and high-Γ regimes in the simulations of Ref. [50] correspond to the same shaking strength [$S = \Gamma(A/d) =$ constant] but having small and large A/d, respectively.) To isolate the possible effects of the two-dimensionality of our experiments on height oscillations, additional experiments (not shown) were conducted in a quasi-2D box (of width of about 5 particle diameter, $W/d = 5.5$, and length $L/d = 100$) with a shallow granular layer ($F = h_0/d = 6$); increasing the shaking intensity from 30 to 40, however, we found that the Leidenfrost state remains a period-1 wave, implying that the LS is synchronized with the shaking frequency even in a quasi-2D vibrofluidized bed. Simulations in a 2D box and/or additional experiments may help to resolve the disagreement between the above simulations [47,50] and our experiments about the synchronous time dependence of the Leidenfrost state.

V. SUMMARY AND CONCLUSIONS

We carried out detailed experiments on the pattern-formation dynamics in a vertically shaken two-dimensional monolayer granular system. A collection of spherical glass beads was held in a Hele-Shaw-type container of certain length (L) and height (H), having a width (W) such that it can accommodate only one layer of beads across its width ($W/d \approx 1.1$); containers with two different lengths, $L/d = 20$ and 40, were investigated. The particle-filled container was vertically vibrated harmonically, $y = A\sin(2\pi f t)$, via an electromagnetic shaker, where A is the amplitude of shaking and f is its frequency. The experimental results were presented for a wide range of (i) shaking intensities $\Gamma = A\omega^2/g \in (0,55)$, (ii) amplitude ratio $A/d \in (0.1,4)$, and (iii) particle loading or filling height $F = h_0/d$ (where h_0 is the number of particle layers at rest). In addition to showing the raw images and movies of various patterns, the quantitative measurements have been made on (i) the density and granular temperatures and (ii) the pair-correlation functions using particle-tracking algorithms.

For shaking accelerations $\Gamma \leqslant 1$, the granular bed moves with the container base without detaching from it and this is the regime of the solid bed which gave birth to the well-known bouncing-bed state (in which the bed detaches from the base and starts bouncing like a single particle) at $\Gamma > 1$. At $\Gamma \sim O(10)$, the BB state transitioned into the so-called Leidenfrost state [31,38] in which a dense cluster of particles floats over a dilute gaseous layer [8,26,31]. The critical shaking acceleration for the transition from BB to LS was found to have a power-law dependence, $\Gamma_{\rm BB}^{\rm LS} \sim F^{1.217}(A/d)^{-7/8}$, on the particle loading depth ($F = h_0/d$) and the shaking amplitude (A/d). Therefore, the critical shaking strength [$S = \Gamma(A/d)$, which is a measure of the input kinetic energy via shaking] increases weakly with increasing shaking amplitude [$S_{\rm BB}^{\rm LS} \propto (A/d)^{1/8}$] for a specified particle loading F; this result is in contrast to the findings of Eshuis *et al.* [31], who showed $S =$ constant at the BB $\rightarrow$ LS transition. We speculate that the frictional barrier at the front and back walls increases with increasing shaking amplitude which might be responsible for the weak increase of $S_{\rm BB}^{\rm LS}$ with A/d.

Carrying out experiments in a container of larger length $L/d = 40$, we uncovered the complete sequence of bifurcations with increasing Γ: SB (solid bed) to BB (bouncing bed) to LS (Leidenfrost state) to 2-roll convection to 1-roll convection and finally to a granular gas. While the first two transitions (SB $\rightarrow$ BB $\rightarrow$ LS) were also reported previously (by Eshuis *et al.* [31]), the LS $\rightarrow$ convection transition and the convection $\rightarrow$ gas transition are new findings in the context of a monolayer vibrofluidized system at strong shaking. In particular, for a given length of the Hele-Shaw container, the coarsening of a pair of convection rolls leading to the genesis of a single-roll structure (i.e., the multiroll transition) and its subsequent transition to a granular gas were not reported in previous experiments (although a recent simulation study [47] did report on a similar multiroll transition in a quasi-2D box). The shaking strength for the onset of the LS $\rightarrow$ convection transition, $S_{\rm LS}^{\rm con} \sim (A/d)^{0.84}$, is found to increase strongly with increasing shaking amplitude. The latter finding is in contrast to the very weak dependence of the same found in the quasi-2D experiments [36], and the related simulations [47] also indicate that $S_{\rm LS}^{\rm con}$ is almost independent of A/d.

The density and temperature profiles, obtained via particle-tracking algorithms, revealed clear signatures of the transition from the bouncing-bed state to the density-inverted Leidenfrost state. The Leidenfrost state is characterized by three distinct regions: (i) a dilute collisional layer of particles near the vibrating base, (ii) a dense floating cluster above the collisional layer, and (iii) a ballistic layer on the top of the floating cluster (where the particles move around ballistically). While the ballistic layer was also found to exist in the bouncing-bed state (at large shaking strength), the crucial distinction of the LS from the BB state is the existence of the dilute collisional layer that acts as a cushion over which a dense cluster floats [31]. Another distinguishing criterion between LS and BB is that the granular temperature in the BB state is lower near the vibrating base in contrast to the LS for which the maximum temperature occurs near the base. The temperature in both BB and LS was found to be "anisotropic" in the sense that the vertical component (T_y) of temperature is, in general, larger than its horizontal component (T_x). Interestingly, in the LS, the temperature ratio T_x/T_y increased with increasing elevation, and can even exceed unity (i.e., $T_x > T_y$) in its ballistic layer at very strong shaking. We note in passing that the modeling of such anisotropic temperature field would require a continuum theory that goes beyond traditional Navier-Stokes-order hydrodynamics [51,52].

The microstructure within the bouncing-bed and the Leidenfrost state were probed by evaluating the two-dimensional pair-correlation function $g(r,\theta)$ which provided information on the particle configuration (i.e., both the spatial and orientational ordering of particles). The sixfold symmetry of the $g(r,\theta)$ in the BB state was tied to the hexagonally packed crystalline structure of the bed, and the degree of anisotropy of this crystalline state was found to decrease with increasing shaking amplitude (A/d) at a fixed shaking intensity Γ and vice versa. The $g(r,\theta)$ in the collisional layer and the ballistic layer of the LS displayed angular isotropy, and are therefore in a gas-like state. The analysis of the radial distribution function, $g(r) \equiv \langle g(r,\theta)\rangle_\theta$, in the floating-cluster region of the LS revealed a clear liquid-like structure [the blue curve in Fig. 14(d)]. Therefore the floating cluster is indeed in a liquid state, which hovers over a gas-like collisional layer underneath, and this makes the connection with the original Leidenfrost state [31,38] more succinct.

We uncovered an unsteady behavior associated with the Leidenfrost state, wherein the height of the collisional layer (i.e., the interface that separates the floating cluster from the dilute collisional layer underneath) as well as the height of the floating cluster oscillated sinusoidally with time. The oscillation frequencies closely matched the frequency of the shaker. Therefore, the granular Leidenfrost state is not a stationary state; rather it is a period-1 or f wave; i.e., the temporal order of the LS is the same as that of the bouncing-bed state. This finding has important implications for the theoretical analysis [35,40] that has been carried out in the recent past. On the other hand, the recent simulations [47] (in a narrow quasi-3D column) identified a low-frequency oscillation in the density-inverted state which we did not observe in our experiments, presumably due to very low values of the underlying frequency and/or due to the lateral confinement of the vibrated column; these issues require future investigations.

In this work we have restricted our experiments to a relatively narrow aspect ratio ($L/h_0 < 7$) container, and did not observe subharmonic patterns such as $f/2$ undulatory waves, $f/4$ spikes, etc. Such patterns are known to appear [3,30,36,37] in experiments with a large aspect ratio ($L/h_0 > 15$) container for a range of Γ lying between the BB state and the LS, and hence they may be expected in the present 2D setup too if we further increase the length of the container. These experimental issues can be taken up in a future work. A recent simulation work [53] has probed the role of noise on the LS $\rightarrow$ convection transition, and modeled it via a quintic-order stochastic amplitude equation. It may be possible to derive such a quintic-order equation from the underlying hydrodynamic equations [54–58]. Lastly, we recall that the theoretical works on granular convection based on linear and nonlinear stability analyses [35,40] do not show any dependence of the critical shaking strength $S_{\rm LS}^{\rm con}$ (for the onset of convection) on the shaking amplitude A/d [in contrast to present findings, Eq. (12)]. This may be due to the oversimplified boundary conditions imposed at the vibrating wall (constant temperature) in all theoretical analyses. Therefore, the present work also opens up important theoretical issues that need to be addressed in the future. Lastly, it would be interesting to investigate the related pattern-formation dynamics in a binary granular mixture [39,59] under harmonic shaking. Works along these directions are in progress.

ACKNOWLEDGMENTS

This work has been generously funded by the Department of Atomic Energy, Government of India, via "DAE-Science Research Council (SRC) Outstanding Research Investigator Award" to M.A. (Project No. 2010/21/06-BRNS). We sincerely thank Krishnoji Rao for fabricating the experimental setup and the related accessories, and Mr. Raghavendra and Mr. Venkateshulu (Jost Engineering Company Ltd.) and Mr. Ramakrishna (Data Physics Pvt. Ltd.) for tutoring I.H.A. on the shaker system. We also thank Dr. Nandu Gopan for assistance with Figs. 7(c), 7(d), and 15.

The experiments and data analysis were carried out by I.H.A. under the supervision of M.A.; the final manuscript and its revision were prepared by M.A.

[1] E. F. F. Chladni, *Entdeckungen über die Theorie des Klanges* (Kessinger, 1787).

[2] M. Faraday, On a peculiar class of acoustic figures and certain forms assumed by a group of particles upon vibrating elastic surfaces, Philos. Trans. R. Soc. London **52**, 299 (1831).

[3] S. Douady, S. Fauve, and C. Laroche, Subharmonic instabilities and defects in a granular layer under vertical vibrations, Europhys. Lett. **8**, 621 (1989).

[4] E. Clement and J. Rachenbach, Fluidization of a bidimensional powder, Europhys. Lett. **16**, 133 (1991).

[5] J. A. C. Gallas, H. J. Herrmann, and S. Sokolowski, Convection Cells in Vibrating Granular Media, Phys. Rev. Lett. **69**, 1371 (1992).

[6] H. K. Pak and R. P. Behringer, Surface Waves in Vertically Vibrated Granular Materials, Phys. Rev. Lett. **71**, 1832 (1993).

[7] S. Luding, E. Clement, A. Blumen, J. Rachenbach, and J. Duran, The onset of convection in molecular dynamics simulations of grains, Phys. Rev. E **50**, R1762 (1994).

[8] Y. Lan and A. D. Rosato, Macroscopic behavior of vibrating beds of smooth inelastic spheres, Phys. Fluids **7**, 1818 (1995).

[9] T. Pöschel and H. J. Herrmann, Size segregation and convection, Europhys. Lett. **29**, 123 (1995).

[10] M. Bourzutschky and J. Miller, Granular Convection in a Vibrated Fluid, Phys. Rev. Lett. **74**, 2216 (1995).

[11] H. Hayakawa, S. Yue, and D. C. Hong, Hydrodynamic Description of Granular Convection, Phys. Rev. Lett. **75**, 2328 (1995).

[12] S. Warr, J. M. Huntley, and G. T. H. Jacques, Fluidization of a two-dimensional granular system: Experimental study and scaling behavior, Phys. Rev. E **52**, 5583 (1995).

[13] C. R. Wassgren, C. E. Brennen, and M. L. Hunt, Vertical vibration of a deep bed of granular materials in a container, J. Appl. Mech. **63**, 712 (1996).

[14] K. M. Aoki, T. Akiyama, Y. Maki, and T. Watanabe, Convective roll patterns in vertically vibrated beds of granules, Phys. Rev. E **54**, 874 (1996).

[15] J. B. Knight, E. E. Ehrichs, V. Y. Kuperman, J. K. Flint, H. M. Jaeger, and S. R. Nagel, Experimental study of granular convection, Phys. Rev. E **54**, 5726 (1996).
[16] P. B. Umbanhower, F. Melo, and H. L. Swinney, Localized excitations in a vertically vibrated granular layer, Nature (London) **382**, 793 (1996).
[17] A. Kudrolli, M. Wolpert, and J. P. Gollub, Cluster Formation due to Collisions in Granular Materials, Phys. Rev. Lett. **78**, 1383 (1997).
[18] C. Bizon, M. D. Shattuck, J. B. Swift, W. D. McCormick, and H. L. Swinney, Patterns in 3D Vertically Oscillated Granular Layers: Simulation and Experiment, Phys. Rev. Lett. **80**, 57 (1998).
[19] R. Ramirez, D. Risso, and P. Cordero, Thermal Convection in Fluidized Granular Systems, Phys. Rev. Lett. **85**, 1230 (2000).
[20] S. C. Yang and S. S. Hsiau, Simulation study of the convection cells in a vibrated granular bed, Chem. Eng. Sci. **55**, 3627 (2000).
[21] T. Pöschel, T. Schwager, and C. Saluena, Onset of fluidization in vertically shaken granular material, Phys. Rev. E **62**, 1361 (2000).
[22] R. D. Wildman, J. M. Huntley, and D. J. Parker, Convection in Highly Fluidized Three-Dimensional Granular Beds, Phys. Rev. Lett. **86**, 3304 (2001).
[23] J. J. Brey, M. J. Ruiz-Montero, and F. Moreno, Hydrodynamics of an open vibrated granular system, Phys. Rev. E **63**, 061305 (2001).
[24] N. Burtally, P. J. King, and M. R. Swift, Spontaneous air-driven separation in vertically vibrated fine granular mixtures, Science **295**, 1877 (2002).
[25] A. Garcimartín, D. Maza, J. L. Ilquimiche, and I. Zuriguel, Convective motion in a vibrated granular layer, Phys. Rev. E **65**, 031303 (2002).
[26] B. Meerson, T. Pöschel, and Y. Bromberg, Close-Packed Floating Clusters: Granular Hydrodynamics beyond a Freezing Point?, Phys. Rev. Lett. **91**, 024301 (2003).
[27] T. Ohtsuki and T. Ohsawa, Hydrodynamics for convection in vibrating beds of cohesionless granular materials, J. Phys. Soc. Jpn. **72**, 1963 (2003).
[28] E. Khain and B. Meerson, Onset of granular convection in a horizontal layer of granular gas, Phys. Rev. E **67**, 021306 (2003).
[29] C. Huan, X. Yang, D. Candela, R. W. Mair, and R. L. Walsworth, NMR experiments on a three-dimensional vibrofluidized granular medium, Phys. Rev. E **69**, 041302 (2004).
[30] O. Sano, Dilatancy, buckling, and undulations on a vertically vibrating granular layer, Phys. Rev. E **72**, 051302 (2005).
[31] P. Eshuis, K. van der Weele, D. van der Meer, and D. Lohse, Granular Leidenfrost Effect: Experiment and Theory of Floating Particle Clusters, Phys. Rev. Lett. **95**, 258001 (2005).
[32] J. A. Carrillo, T. Pöschel, and C. Saluena, Granular hydrodynamics and pattern formation in vertically oscillated granular disk layers, J. Fluid Mech. **597**, 119 (2007).
[33] A. Kudrolli, Size separation in vibrated granular materials, Rep. Prog. Phys. **67**, 209 (2004).
[34] I. S. Aranson and L. S. Tsimring, Patterns and collective behavior in granular media: Theoretical concepts, Rev. Mod. Phys. **78**, 641 (2006).
[35] P. Shukla, I. Ansari, D. van der Meer, D. Lohse, and M. Alam, Nonlinear instability and convection in a vertically vibrated granular bed, J. Fluid Mech. **761**, 123 (2014).
[36] P. Eshuis, K. van der Weele, D. van der Meer, R. Bos, and D. Lohse, Phase diagram of vertically shaken granular matter, Phys. Fluids **19**, 123301 (2007).
[37] I. Ansari and M. Alam, Patterns and velocity field in vertically vibrated granular materials, AIP Conf. Proc. **1542**, 775 (2013).
[38] J. G. Leidenfrost, *De Aquae Communis Nonnullis Qualitatibus Tractatus* (University of Duisburg, Duisburg, Germany, 1756).
[39] I. Ansari and M. Alam, Patterns, segregation, and hysteresis in vertically vibrated granular mixtures, Bull. Am. Phys. Soc. **57**, 358 (2012).
[40] P. Eshuis, K. van der Weele, M. Alam, H. J. van Gerner, K. van der Weele, and D. Lohse, Onset of Convection in Strongly Shaken Granular Matter, Phys. Rev. Lett. **104**, 038001 (2010).
[41] P. Eshuis, D. van der Meer, M. Alam, H. J. van Gerner, M. van der Hoef, H. Kuipers, S. Luding, D. van der Meer, and D. Lohse, Buoyancy driven convection in vertically shaken granular matter: Experiments, numerics, and theory, Granular Matter **15**, 893 (2013).
[42] J. C. Crocker and D. Grier, Methods of digital video microscopy for colloidal studies, J. Coll. Interface Sci. **179**, 298 (1996).
[43] I. F. Sbalzarini and P. Koumoutsakos, Feature point tracking and trajectory analysis for video imaging in cell imaging, J. Struc. Biol. **151**, 182 (2005).
[44] Dantec Dynamics A/S product information on adaptive correlation in dynamic studio, http://www.dantecdynamics.com.
[45] F. Scarano and R. L. Riethmuller, Advances in iterative multigrid PIV image processing, Exp. Fluids **29**, S51 (2000).
[46] See Supplemental Material at http://link.aps.org/supplemental/10.1103/PhysRevE.93.052901 for three movies showing convection patterns as in Figs. 7(c) and 7(d).
[47] N. Rivas, S. Luding, and A. R. Thornton, Low-frequency oscillations in narrow vibrated granular systems, New J. Phys. **15**, 113043 (2013).
[48] M. P. Allen and D. J. Tildesley, *Computer Simulations of Liquids* (Clarendon, Oxford, 1989).
[49] T. V. Bogdan, Atom-atomic potentials and the correlation distribution functions for modeling liquid benzene by molecular dynamics methods, Russian J. Phys. Chem. **80**, 14 (2006).
[50] J. Bougie, V. Policht, and J. K. Pearce, Time dependence and density inversion in simulations of vertically oscillated granular layers, Phys. Rev. E **86**, 020302(R) (2012).
[51] S. Saha and M. Alam, Non-Newtonian stress, collisional dissipation, and heat flux in the shear flow of inelastic disks: A reduction via Grad's moment method, J. Fluid Mech. **757**, 251 (2014).
[52] S. Saha and M. Alam, Normal stress differences, their origin, and constitutive relations for a sheared granular fluid, J. Fluid Mech. **795**, 549 (2016).
[53] N. Rivas, A. R. Thornton, S. Luding, and D. van der Meer, From the granular Leidenfrost state to buoyancy-driven convection, Phys. Rev. E **91**, 042202 (2015).
[54] P. Shukla and M. Alam, Nonlinear vorticity-banding instability in granular plane Couette flow: Higher-order Landau coefficients, bistability, and the bifurcation scenario, J. Fluid Mech. **718**, 131 (2013).

[55] M. Alam and P. Shukla, Nonlinear stability, bifurcation, and vortical patterns in three-dimensional granular plane Couette flow, J. Fluid Mech. **716**, 349 (2013).

[56] P. Shukla and M. Alam, Nonlinear stability and patterns in granular plane Couette flow: Hopf and pitchfork bifurcations, and evidence for resonance, J. Fluid Mech. **672**, 147 (2011).

[57] P. Shukla and M. Alam, Weakly nonlinear theory of shear-banding instability in granular plane Couette flow: Analytical solution, comparison with numerics, and bifurcation, J. Fluid Mech. **666**, 204 (2011).

[58] P. Shukla and M. Alam, Landau-type Order Parameter Equation for Shear Banding in Granular Couette Flow, Phys. Rev. Lett. **103**, 068001 (2009).

[59] I. Ansari, N. Rivas, and M. Alam, Phase-coexisting patterns with segregation and controlled convection in vertically vibrated binary granular mixtures (unpublished).